Time-Dependent Response of a Two-Dimensional Airfoil in Transonic Flow

D. P. Rizzetta*
Air Force Flight Dynamics Laboratory, Wright-Patterson AFB, Ohio

A procedure is developed for the aeroelastic analysis of a two-dimensional airfoil in transonic flow. The fluid is assumed to be described by the unsteady low-frequency small-disturbance transonic potential equation for which a fully time-implicit integration scheme exists. Structural equations of motion are integrated in time simultaneously with the potential equation in order to predict the unsteady airfoil motion. As a computational example, a three-degree-of-freedom NACA 64A010 airfoil is considered using representative values of the structural parameters. The method is shown to be both stable and accurate, and the time response for several choices of initial conditions and reduced freestream density is presented. Oscillations with either growing or decaying amplitudes are indicated depending upon the prescribed initial conditions.

Introduction

FOR the case of flow over an airfoil in a freestream at Mach numbers near 1, small amplitude motions of the body surface can produce large variations in the aerodynamic forces and moments acting on the structure. In addition, phase differences between the flow variables and the resultant forces may be great. These characteristics tend to enhance the probability of encountering aeroelastic instabilities in the transonic flow regime, and thus evidence a need for techniques of analyzing the coupled unsteady flowfield and resultant structural response in such situations.

In the subsonic and supersonic cases, the governing flow equations may be linearized such that the aerodynamic forces depend upon the body motion in a linear fashion. Moreover, the resultant forces acting on the airfoil may be obtained through superposition by summing the contributions due to each of the various types of body motion permitted. This allows the linear structural equations of motion to be solved independent of the governing aerodynamic equations which provide only the force coefficients. Uncoupling of the fluid and structural equations is not, in general, possible for the transonic regime due to its inherent nonlinear nature.

Recent advances in computational methods have made several approaches available for computing unsteady transonic flows. While a number of different techniques have evolved and various physical problems have been considered,[1-16] the unsteady body motion was generally prescribed as a known function of time, thereby precluding the simulation of true aeroelastic behavior. Only more recently have these procedures been applied to actual aeroelastic problems.[17,18] It is the intent here to describe a method for obtaining the time-dependent response of a two-dimensional airfoil in transonic flow and to provide a computational example by applying this technique to a physical situation of practical interest.

The governing aerodynamic equation of motion is assumed to be the unsteady low-frequency small-disturbance transonic equation for the velocity potential function which is capable of simulating nonlinear flow phenomena including irregular shock wave motions. Solutions to this equation have compared well with solutions of the unsteady Euler equations[15] and have predicted behavior which has commonly been observed experimentally. In addition, a fully time-implicit method of integrating this equation already exists. Structural equations of motion for a three-degree-of-freedom airfoil are formulated by modeling the structure as a spring-mass system. The coupled aerodynamic and structural equations are then integrated in time such that the flowfield and the response of the airfoil to the resultant aerodynamic forces are allowed to interact in a manner much like the physical situation.

The method of time integration has previously been applied in a superficial manner for an aeroelastic calculation. In Ref. 17, several types of motion for a simple one-degree-of-freedom airfoil were shown to result by varying the structural parameters. While the approach here is considered a direct extension of that effort, an alternative point of view is taken. The structural parameters are presumed fixed and the motion resulting from several choices of the initial conditions and reduced freestream density is considered. Because of the nonlinear equation for the velocity potential, oscillations with either growing or decaying amplitudes may be produced solely by the choice of initial conditions.

Governing Equations

The airfoil of chord c, linear mass distribution $m(x)$, and maximum thickness to chord ratio δ is depicted in Fig. 1. If K_σ, K_α, and K_β are the respective spring constants, D_σ, D_α, and D_β the respective damping coefficients for assumed uncoupled damping, and C_l, C_{mo}, and C_{mh} the force coefficients, then the physical equations for the spring-mass system are the following:[19]

$$M\frac{d^2h}{dt^2}+S_\alpha\frac{d^2\alpha}{dt^2}+S_\beta\frac{d^2\beta}{dt^2}+D_\sigma\frac{dh}{dt}+K_\sigma h=\rho_\infty u_\infty^2 c^2 C_l(t)/2 \tag{1a}$$

$$S_\alpha\frac{d^2h}{dt^2}+I_\alpha\frac{d^2\alpha}{dt^2}+[(x_o-x_h)S_\beta+I_\beta]\frac{d^2\beta}{dt^2}+D_\alpha\frac{d\alpha}{dt}+K_\alpha\alpha=\rho_\infty u_\infty^2 c^3 C_{mo}(t)/2 \tag{1b}$$

$$S_\beta\frac{d^2h}{dt^2}+[(x_o-x_h)S_\beta+I_\beta]\frac{d^2\alpha}{dt^2}+I_\beta\frac{d^2\beta}{dt^2}+D_\beta\frac{d\beta}{dt}+K_\beta\beta=\rho_\infty u_\infty^2 c^3 C_{mh}(t)/2 \tag{1c}$$

Received Jan. 11, 1978; revision received Aug. 31, 1978.

Index categories: Nonsteady Aerodynamics; Transonic Flow; Structural Dynamics.

*Visiting Scientist, Analysis and Optimization Branch, Structural Mechanics Division; presently, Specialist Engineer, The Boeing Company, Seattle, Wash. Member AIAA.

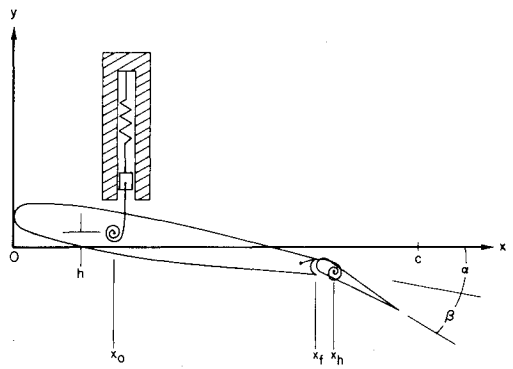

Fig. 1 Airfoil with plunge, pitch and aileron degrees of freedom.

where

$$M=\int_0^c m(x)\,dx \tag{2}$$

$$S_\alpha=\int_0^c (x_o-x)\,m(x)\,dx \tag{3a}$$

$$S_\beta=\int_{x_f}^c (x_h-x)\,m(x)\,dx \tag{3b}$$

$$I_\alpha=\int_0^c (x_o-x)^2 m(x)\,dx \tag{4a}$$

and

$$I_\beta=\int_{x_f}^c (x_h-x)^2 m(x)\,dx \tag{4b}$$

These can be put into a nondimensional form which will be compatible with the velocity potential equation by defining

$$\xi=x/c \tag{5}$$

$$\tau=u_\infty \delta^{2/3} t/c \tag{6}$$

$$\sigma=h/c \tag{7}$$

$$\bar{\xi}_o=S_\alpha/cM \tag{8a}$$

$$\bar{\xi}_f=S_\beta/cM \tag{8b}$$

$$\xi_o^*=I_\alpha/c^2M \tag{9a}$$

$$\xi_f^*=I_\beta/c^2M \tag{9b}$$

$$\omega_\sigma=(c^2K_\sigma/u_\infty^2M)^{1/2} \tag{10a}$$

$$\omega_\alpha=(K_\alpha/u_\infty^2\xi_o^*M)^{1/2} \tag{10b}$$

$$\omega_\beta=(K_\beta/u_\infty^2\xi_f^*M)^{1/2} \tag{10c}$$

$$\zeta_\sigma=cD_\sigma/2u_\infty\omega_\sigma M \tag{11a}$$

$$\zeta_\alpha=c\xi_o^*D_\alpha/2u_\infty\omega_\alpha I_\alpha \tag{11b}$$

$$\zeta_\beta=c\xi_f^*D_\beta/2u_\infty\omega_\beta I_\beta \tag{11c}$$

and

$$\mu=2M/\rho_\infty c^3 \tag{12}$$

If these equations are substituted into Eqs. (1), then the following equations result:

$$\sigma''(\tau)+\bar{\xi}_o\alpha''(\tau)+\bar{\xi}_f\beta''(\tau)+2\delta^{-2/3}\omega_\sigma\zeta_\sigma\sigma'(\tau)+\delta^{-4/3}\omega_\sigma^2\sigma(\tau)=\delta^{-4/3}C_l(\tau)/\mu \tag{13a}$$

$$\bar{\xi}_o\sigma''(\tau)+\xi_o^*\alpha''(\tau)+[(\xi_o-\xi_n)\bar{\xi}_f+\xi_f^*]\beta''(\tau)+2\delta^{-2/3}\omega_\alpha\zeta_\alpha\alpha'(\tau)+\delta^{-4/3}\xi_o^*\omega_\alpha^2\alpha(\tau)=\delta^{-4/3}C_{mo}(\tau)/\mu \tag{13b}$$

$$\bar{\xi}_f\sigma''(\tau)+[(\xi_o-\xi_h)\bar{\xi}_f+\xi_f^*]\alpha''(\tau)+\xi_f^*\beta''(\tau)+2\delta^{-2/3}\omega_\beta\zeta_\beta\beta'(\tau)+\delta^{-4/3}\xi_f^*\omega_\beta^2\beta(\tau)=\delta^{-4/3}C_{mh}(\tau)/\mu \tag{13c}$$

This system may be written as the vector equation

$$\mathfrak{M}X''(\tau)+\mathfrak{D}X'(\tau)+\mathfrak{K}X(\tau)=C(\tau)/\mu \tag{14}$$

such that the solution to Eq. (14) with initial conditions $X(0)$ and $X'(0)$ provide the unsteady airfoil response.

If the flow is assumed to be irrotational, the Mach number near 1, δ small, and only low-frequency unsteady disturbances are considered, then a simple equation for the perturbation velocity potential function results. This is the low-frequency small-disturbance equation[20] which is the leading order result for transonic flow and will be used here in the nondimensional form

$$[(1-M_\infty^2)\delta^{-2/3}-(1+\gamma)M_\infty^2\phi_\xi]\phi_{\xi\xi}+\phi_{\eta\eta}=2M_\infty^2\phi_{\xi\tau} \tag{15}$$

Boundary conditions for Eq. (15) are obtained from flow tangency on the airfoil surface, from the Kutta condition at the trailing edge with a constant jump in potential across the vortex sheet in the wake, and by requiring the perturbation velocity to vanish at infinity. The airfoil geometry may be described by

$$y=c\delta f(\xi) \tag{16}$$

such that the surface boundary condition becomes

$$\phi_\eta=f'(\xi)-\alpha(\tau)/\delta \qquad \text{for } 0\le\xi<\xi_f \tag{17a}$$

$$\phi_\eta=f'(\xi)-\alpha(\tau)/\delta-\beta(\tau)/\delta \qquad \text{for } \xi_f\le\xi\le 1 \tag{17b}$$

where Eqs. (17) are applied on $\eta=0^\pm$ as is consistent with the small-disturbance assumption. It is noted that to the order considered in Eq. (15) there is no explicit dependence upon σ appearing in the surface boundary condition. The solution of Eq. (15) with corresponding boundary conditions and initial profile $\phi(\xi,\eta,0)$ provides a complete flowfield description. The resultant local unsteady pressure coefficient is then given by

$$C_p=-2\delta^{2/3}\phi_\xi \tag{18}$$

from which the airfoil lift and moment coefficients may be obtained as

$$C_l=\int_0^1 (C_{p^-}-C_{p^+})\,d\xi \tag{19}$$

$$C_{mo}=\int_0^1 (C_{p^-}-C_{p^+})(\xi_o-\xi)\,d\xi \tag{20a}$$

$$C_{mh}=\int_{\xi_f}^1 (C_{p^-}-C_{p^+})(\dot{\xi}_h-\xi)\,d\xi \tag{20b}$$

Method of Solution

We now indicate a method for obtaining solutions to the coupled aeroelastic system Eq. (14) with specified initial conditions and Eq. (15) with appropriate boundary conditions and initial profile $\phi(\xi,\eta,0)$. Equation (14) is written as an equivalent first-order system with

$$X_1(\tau) = X(\tau) \tag{21a}$$

$$X_2(\tau) = X'(\tau) \tag{21b}$$

such that

$$X_1'(\tau) = X_2(\tau) \tag{22a}$$

and

$$X_2'(\tau) = \mathfrak{M}^{-1}[C(\tau)/\mu - \mathfrak{D}X_2(\tau) - \mathfrak{K}X_1(\tau)] \tag{22b}$$

This system is then integrated in time by a four-point Adams-Moulton[21] implict predictor-corrector scheme having a local truncation error of order $(\Delta\tau)^4$. A number of other methods, both explicit and implicit, were tried. It was found that when coupled with the aerodynamic equation (from which $C(\tau)$ is obtained), calculations eventually became unstable for central difference and three-term Taylor series explicit schemes and for Euler-Cauchy and Milne three-point implicit schemes, even when extremely small time step sizes were employed. A Milne five-point implicit method with local truncation error of order $(\Delta\tau)^6$, although stable, appeared to produce less accuracy than the Adams-Moulton integration. No attempt was made here to obtain normal modes for the airfoil response as this is not, in general, possible for arbitrary values of the mass, damping, and stiffness matrices $(\mathfrak{M},\mathfrak{D},\mathfrak{K})$.[22]

For comparison with the time-integrated results of Eqs. (22) it will be of interest to consider homogeneous solutions of the structural system. In particular, for $\mu \to \infty$ the homogeneous result should be recovered. For $C(\tau) = 0$ solutions to Eqs. (22) were obtained from the associated eigenvalue problem. These solutions are thus considered "exact" as they are free of the truncation error which is present in time-integrated results.

An efficient time-implicit finite-difference algorithm has been developed for obtaining solutions to the low-frequency transonic equation. This technique was incorporated in the computer code LTRAN2 developed by Ballhaus and Goorjian[15] for the purpose of computing unsteady transonic flows over airfoils using Eq. (15). Details of LTRAN2 will be briefly summarized here, but for a more complete description the reader is referred to Ref. 15.

The basic LTRAN2 code employs a noniterative alternating-direction implicit (ADI) scheme to advance the solution for ϕ from one time step to the next at each grid point in the computational flowfield. Differencing in the ξ direction is of the mixed type, which has been quite successful in maintaining stability for both subsonic and supersonic flow regions in the case of steady transonic flows.[23] Conservative differencing of the equation is preserved, which is essential for a proper description of shock wave motions. While the ADI scheme has no time-step limitation for stability based upon classical linear stability analysis, instabilities may be generated by the motion of shock waves due to the mixed differencing. Thus $\Delta\tau$ must be chosen such that shock waves do not travel more than one mesh point in the ξ direction over a single time step. Mesh boundaries are taken sufficiently far from the airfoil such that the perturbation velocity approaches zero there. For this purpose a smooth nonuniform computational mesh which is symmetric about $\eta = 0$ is employed. The grid spacing is such that mesh points are clustered near the airfoil leading and trailing edges in the ξ direction and near $\eta = 0$ in the η direction. For all of the results presented here, 99 ξ-points with 33 lying on the airfoil and 79 η-points were used to form the computational flowfield. Minimum grid spacings were taken as $\Delta\xi_{\min} = 0.0033$ and $\Delta\eta_{\min} = 0.0200$ with the computational domain defined by $-1033.5 \le \xi \le 855.9$ and $-811.1 \le \eta \le 811.1$.

In order to incorporate the simultaneous solution of the structural equations, it was necessary to adapt the original LTRAN2 code to accommodate the predictor-corrector integration. The marching technique thus becomes a coupled two-step process. Although this in effect doubles the computing time for fixed $\Delta\tau$, without this modification stable calculations could not, in general, be obtained. Details of implementing this procedure are briefly summarized in the Appendix.

Results

All of the results presented here correspond to an NACA 64A010 airfoil which is 10% thick and representative of transonic airfoils commonly in use. In order to establish the accuracy and stability of the computational method it will be demonstrated that an exact solution of the structural equations can be reproduced by time integration. Using a steady-state profile for $M_\infty = 0.72$ as the initial condition, Eq. (15) alone was integrated in time for three periods of forced oscillation with the airfoil displacements specified according to the prescribed functions

$$\sigma(\tau) = \alpha(\tau) = \beta(\tau) = 0.01745\sin(0.233\tau) \tag{23}$$

corresponding to 1 deg of airfoil and flap oscillation at a reduced frequency $(\omega c/u_\infty)$ of 0.05. After a short period of time the effect of the initial conditions was negligible such that the aerodynamic forces C_l, C_{mo}, and C_{mh} became periodic. The amplitude and phase for each force was extracted from the numerical results and introduced into Eqs. (22). Structural parameters comprising the mass, damping, and stiffness matrices and reduced density μ were then chosen such that Eq. (23) represented the solution of the structural system. At this point the combined aeroelastic equations were integrated in time using as initial conditions the values which had evolved when forced motion was terminated. Results of this procedure are shown in Fig. 2 in terms of the unsteady lift, which was found to be most sensitive to numerical instabilities. For three periods of free oscillation the variation in C_l was never more than 0.5% and it appeared that the integration could have proceeded indefinitely without instability or loss of accuracy.

We now consider solutions of the coupled aeroelastic equations for representative choices of the structural parameters. Impulsive motion from an initial equilibrium state will be the only type of motion considered here, corresponding to the initial conditions

$$\sigma(0) = \alpha(0) = \beta(0) = \sigma'(0) = \beta'(0) = 0 \tag{24a}$$

$$\alpha'(0) \text{ prescribed} \tag{24b}$$

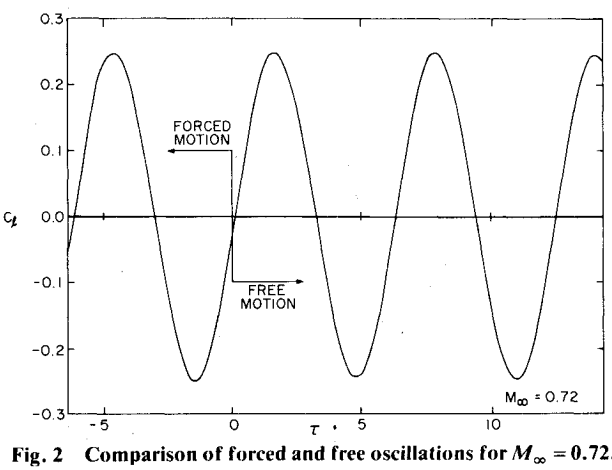

Fig. 2 Comparison of forced and free oscillations for $M_\infty = 0.72$.

with $\phi(\xi,\eta,0)$ given by the steady-state profile for $M_\infty = 0.82$. The initial surface pressure distribution for this case is shown in Fig. 3 where it is noted that a shock is present between $\xi = 0.5$ and $\xi = 0.6$. The airfoil pitch point, aileron leading-edge location, and aileron pitch point, respectively, were selected as $\xi_o = 0.25$, $\xi_f = 0.75$, and $\xi_h = 0.80$. Non-dimensional mass moments were chosen to be the following:

$$\bar{\xi}_o = -0.1818, \quad \bar{\xi}_f = -0.0034 \tag{25a}$$

$$\xi_o^* = 0.1141, \quad \xi_f^* = 0.0346 \tag{25b}$$

By way of comparison, if the airfoil is assumed to consist of a homogeneous material of uniform density, then it may be shown that

$$\bar{\xi}_o = -0.1818, \quad \bar{\xi}_f = -0.0034 \tag{26a}$$

$$\xi_o^* = 0.0846, \quad \xi_f^* = 0.0052 \tag{26b}$$

Damping coefficients and reduced frequencies were selected as

$$\zeta_\sigma = \zeta_\alpha = \zeta_\beta = 0.03 \tag{27a}$$

$$\omega_\sigma = 0.1, \quad \omega_\alpha = 0.2, \quad \omega_\beta = 0.3 \tag{27b}$$

In terms of the physical system these parameters correspond to the relationships

$$D_\alpha / D_\beta = 2/3, \quad D_\alpha / c^2 D_\sigma = 2 \tag{28a}$$

$$K_\alpha / K_\beta \approx 1.5, \quad K_\alpha / c^2 K_\sigma \approx 0.5 \tag{28b}$$

which are considered typical for aeroelastic applications.

For all calculations the time step size $\Delta\tau$ was specified to be 0.01745 which is equivalent to 360 time steps per period of oscillation at a reduced frequency of 0.215. This represents one chord length of airfoil travel in 12.344 time steps. Time accuracy of the solutions was further confirmed by doubling this nominal value of $\Delta\tau$ and comparing with previous results. It was found that solutions agreed to three significant figures of accuracy in all dependent variables, even for the most severe cases. When the time increment was increased by a factor of five times the nominal value, however, computations eventually became unstable. This was most likely due to a violation of the time step size limitation with respect to the shock wave motion across the computational mesh which has been previously described. All calculations were performed on a CDC Cyber 74 system and required approximately 20 min of central processing time for every 1000 time steps.

Solutions for the initial condition $\alpha'(0) = 0.01745$, 0.05235, and 0.08725 will be considered. In dimensional units of degrees ($180\,\alpha'(0)/\pi$) these choices correspond to $\alpha'(0) = 1$, 3, and 5, respectively. For the reduced density, the values $\mu = 1430$, 2860, and 5730 were prescribed. These correspond to $\mu = 25$, 50, and 100, respectively, in units of inverse degrees ($\pi\mu/180$). For convenience, all further reference to prescribed values of $\alpha'(0)$ and μ will be made in terms of the indicated dimensional quantities.

Unsteady airfoil displacements for the initial condition $\alpha'(0) = 1$ and several values of reduced density appear in Fig. 4 where the homogeneous solution is provided for comparison. For small τ the displacements reproduce the homogeneous result because of the initial equilibrium state. As μ decreases, corresponding to greater aerodynamic loading on the airfoil, the time-integrated results are seen to vary slowly from the homogeneous solution. For μ greater than about 200 the homogeneous result was recovered intact by integrating in time thus assuring accuracy of the numerical

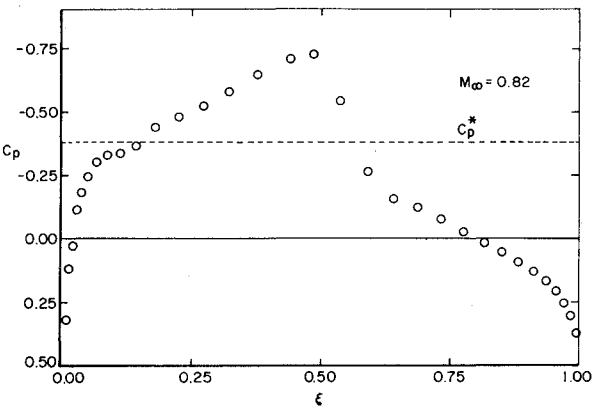

Fig. 3 Initial surface pressure distribution for $M_\infty = 0.82$.

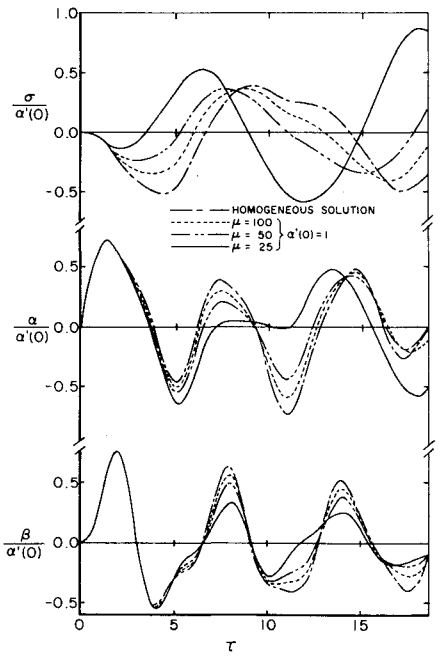

Fig. 4 Unsteady airfoil displacements for $\alpha'(0) = 1$.

method. The displacements are seen to undergo a shift in frequency for decreasing μ which is most noticeable in the plunge. Solutions for $\mu = 100$ and $\mu = 50$ are damped in time compared to the homogeneous result, while growing oscillations are produced in the plunge and airfoil pitching displacement for $\mu = 25$. The aileron pitching displacement appears to be damped for all values of μ. Corresponding aerodynamic coefficients for these cases are given in Fig. 5 where it is seen that they behave in a manner which is quite similar to that of the displacements. Over 1000 time steps were used to generate the solutions appearing in these figures.

Unsteady displacements for $\mu = 25$ and several values of $\alpha'(0)$ are shown in Fig. 6. These are now compared with the undamped homogeneous solution (i.e., $\zeta_\sigma = \zeta_\alpha = \zeta_\beta = 0$). It has already been indicated that with $\mu = 25$ and $\alpha'(0) = 1$ growing amplitudes of some displacements were indicated when compared to the homogeneous result. But as the homogeneous solution is in itself damped, unless the ζ_i's $= 0$, this may be misleading especially because of the several superimposed modes which are present in the solution for any one of the displacements. The long-time behavior can always be deduced by integrating sufficiently far in time, but this may prove costly. If it is only desired to establish whether oscillations are growing or damped by observing the relatively small-time response, then comparison with the undamped homogeneous solution may be quite useful.

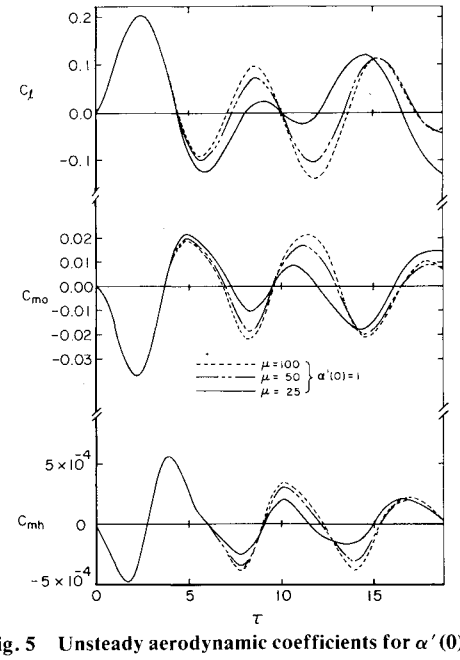

Fig. 5 Unsteady aerodynamic coefficients for $\alpha'(0) = 1$.

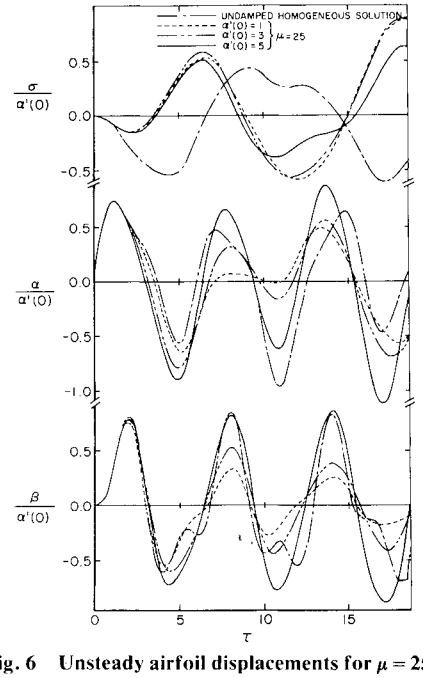

Fig. 6 Unsteady airfoil displacements for $\mu = 25$.

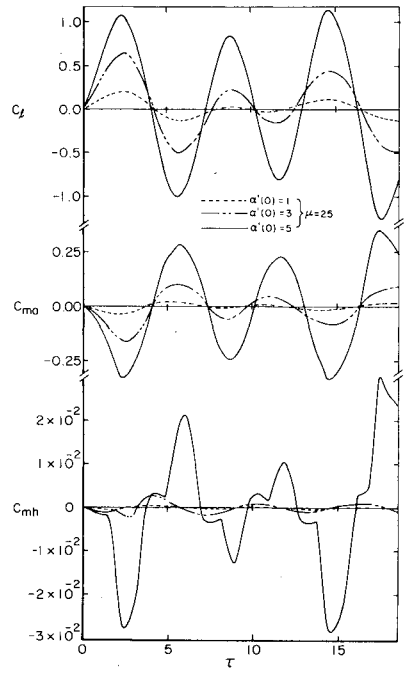

Fig. 7 Unsteady aerodynamic coefficients for $\mu = 25$.

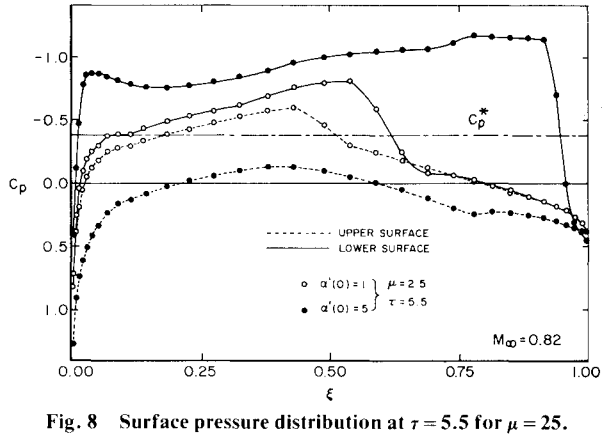

Fig. 8 Surface pressure distribution at $\tau = 5.5$ for $\mu = 25$.

Figure 6 indicates growing plunge oscillations for all values of the initial condition with little change in frequency as $\alpha'(0)$ is varied. For the airfoil and aileron pitching displacements, only the case $\alpha'(0) = 5$ appears to cause undamped motion. The unsteady aerodynamic coefficients for these cases are shown in Fig. 7. Once again the behavior is similar to that of the displacements. The abrupt changes in slope of the aileron moment coefficient are due to the unsteady motion of the shock wave passing across the control surface. This is evident from the surface pressure distribution shown in Fig. 8 for $\tau = 5.5$. The time here corresponds approximately to relative maximums in the airfoil and aileron moments and a relative minimum in the lift. For $\alpha'(0) = 5$, the entire upper surface is now subcritical while most of the lower surface has become supercritical with the shock located near the trailing edge. It will be recalled that in the initial profile a shock was present on both surfaces near midchord (see Fig. 3). By comparison, for the case $\alpha'(0) = 1$ the shock is displaced only slightly forward on the upper surface and only slightly aft on the lower surface from its initial position. This type of shock wave motion is representative of that which can be simulated by the low-frequency transonic equation.

As an example of the long-time behavior of the airfoil response, integration for the case $\mu = 25$ and $\alpha'(0) = 5$ was carried out for over 3000 time steps. Results of this extended time history for the displacements appear in Fig. 9 where it is now clearly seen that all exhibit increasing amplitudes. For the aerodynamic coefficients shown in Fig. 10, irregular behavior is beginning to appear when the displacement amplitudes become large because of the increasing shock strength and its motion. It should be noted, however, that for very large time the displacements are so great that the small-disturbance assumptions may have been violated. Large time results in general should be regarded with caution due to the accumulation of truncation error incurred during the integration process. Time step size studies and the results of the forced-free oscillation study tend to indicate that the solutions presented here may be considered reasonably reliable.

Conclusions and Discussion

While the procedure described here does provide a method for transonic analysis, several issues regarding the

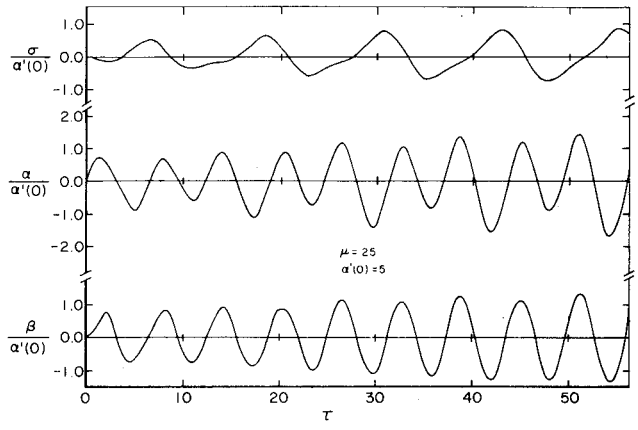

Fig. 9 Extended time history of unsteady airfoil displacements for $\mu = 25$ and $\alpha'(0) = 5$.

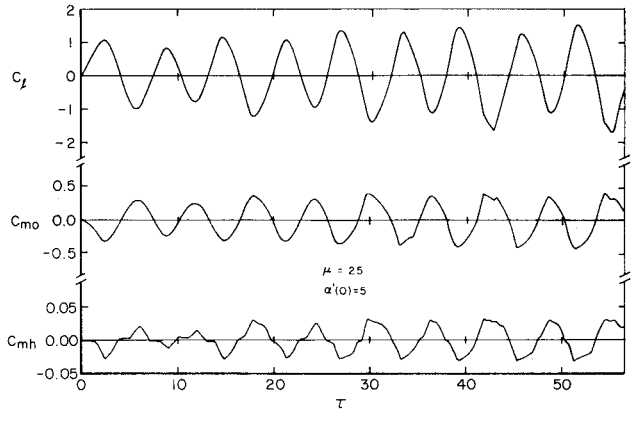

Fig. 10 Extended time history of unsteady aerodynamic coefficients for $\mu = 25$ and $\alpha'(0) = 5$.

physical validity of the results should be addressed. Specifically, the low-frequency approximation may be questioned, particularly for the impulsive motions which have been considered. Strictly speaking, this approximation remains valid only for reduced frequencies of the order of $\delta^{2/3}$. Yet impulsive motions in general permit all frequencies to occur within the solution time domain. Although it is clear then that the results presented here cannot be accurate for very small time, the question of whether or not the neglected higher frequency effects play a role in the long-time aeroelastic stability remains unanswered.

It was noted earlier that there is no explicit dependence upon the airfoil plunge appearing in the unsteady surface boundary condition. While this is consistent with the low-frequency approximation, it does not preclude effects of the plunge mode from determining the overall airfoil response due to the explicit appearance of σ in the coupled aeroelastic system.

For the present calculations, computational boundaries were taken sufficiently far from the airfoil surface such that no reflected disturbances were believed to have contaminated the near-field solution. The work of Ref. 15 indicates that the treatment of the far-field boundary condition (in LTRAN2) is adequate for the types of motion which were considered. This is especially important when obtaining extended time results.

A general procedure has been indicated for the aeroelastic analysis of two-dimensional airfoils in transonic flows. The method has been shown to be both stable and accurate and a computational example for a physical situation of practical interest has been presented. Due to the inherent nonlinearity of the transonic potential equation, various types of motion were found to result depending upon the choice of initial conditions. This is quite unlike classical flutter analysis. Physically, the initial conditions $\sigma'(0)$, $\alpha'(0)$, and $\beta'(0)$ can be interpreted as impulsive gust velocities. By varying these parameters, it may then be possible to establish stability boundaries. Because superposition cannot be applied, however, combinations other than those given by Eq. (24) must necessarily be considered. While this may involve a considerable amount of computation, time integration does provide one method for transonic aeroelastic analysis, including a proper description of nonlinear shock wave motion, which until now has largely been ignored.

Appendix: Time Marching Procedure

The fundamental problem of solving the combined aeroelastic equations is that in order to advance the solution for ϕ from one time level to the next, a time accurate description of the boundary at the new time level is required. But because the boundary at the new time depends itself upon ϕ at the new time, the two must be solved for simultaneously. This was accomplished in the following manner. It was assumed that ϕ, X, and C are known at several previous time levels and it is desired to advance the solution at time τ to time $\tau+\Delta\tau$. The following steps comprise the basic procedure: 1) predict the solution for X at $\tau^* = \tau+\Delta\tau$ based upon C and X at τ; 2) compute ϕ at $\tau^* = \tau+\Delta\tau$ based upon the predicted solution for X at τ^*; 3) obtain C at τ^* resulting from ϕ at τ^*; 4) correct the solution for X at $\tau+\Delta\tau$ based upon C and X at τ^*; 5) recompute ϕ at $\tau+\Delta\tau$ now based upon the corrected solution for X at $\tau+\Delta\tau$; 6) obtain C at $\tau+\Delta\tau$ resulting from ϕ at $\tau+\Delta\tau$.

The solution may now be advanced to the next time level by repeating steps 1-6.

Acknowledgments

The author is grateful to W. F. Ballhaus for making the LTRAN2 code available for his use and also wishes to acknowledge J. J. Olsen and D. W. Quinn for many helpful discussions. This work was supported by the U.S. Air Force under Contract F33615-76-C-3146.

References

[1]Beam, R. M. and Warming, R. F., "Numerical Calculations of Two-Dimensional, Unsteady Transonic Flows with Circulation," NASA TN D-7605, Feb. 1974.

[2]Traci, R. M., Albano, E. D., Farr, J. L., and Cheng, H. K., "Small Disturbance Transonic Flows about Oscillating Airfoils," AFFDL-TR-74-37, June 1974.

[3]Ehlers, F. E., "A Finite Difference Method for the Solution of the Transonic Flow Around Harmonically Oscillating Wings," NASA CR-2257, July 1974.

[4]Magnus, R. J. and Yoshihara, H., "Calculations of Transonic Flow Over an Oscillating Airfoil," AIAA Paper 75-98, Pasadena, Calif., Jan. 1975.

[5]Traci, R. M., Albano, E. D., and Farr, J. L., "Small Disturbance Transonic Flows over Oscillating Airfoils and Planar Wings," AFFDL-TR-75-100, Aug. 1975.

[6]Ballhaus, W. F. and Steger, J. L., "Implicit Approximate-Factorization Schemes for the Low-Frequency Transonic Equation," NASA TM X-73, 082, Nov. 1975.

[7]Ballhaus, W. F., Magnus, R., and Yoshihara, H., "Some Examples of Unsteady Transonic Flow," *Proceedings of the Symposium on Unsteady Aerodynamics*, Vol. II, Arizona Board of Regents, Tucson, Ariz., 1975, pp. 769-791.

[8]Beam, R. M. and Warming, R. F., "An Implicit Finite Difference Algorithm for Hyperbolic Systems in Conservation-Law Form," *Journal of Computational Physics*, Vol. 22, Jan. 1976, pp. 87-110.

[9]Weatherill, W. H., Sabastian, J. D., and Ehlers, F. E., "On the Computation of the Transonic Perturbation Flow Fields Around Two- and Three-Dimensional Oscillating Wings," AIAA Paper 76-99, Washington, D.C., Jan. 1976.

[10]Ballhaus, W. F., "Some Recent Progress in Transonic Flow Computations," VKI Lecture Series: Computational Fluid Dynamics, Rhode-St.-Genese, Belgium, Mar. 1976.

[11]Beam, R. M. and Ballhaus, W. F., "Numerical Integration of the Small-Disturbance Potential and Euler Equations for Unsteady Transonic Flows," NASA SP-347, Part II, March 1976, pp. 789-809.

[12]Caradonna, F. X. and Isom, M. P., "Numerical Calculation of Unsteady Transonic Potential Flow over Helicopter Rotor Blades," *AIAA Journal*, Vol. 14, April 1976, pp. 482-488.

[13]Magnus, R. and Yoshihara, H., "Calculation of the Transonic Oscillating Flap with 'Viscous' Displacment Effects," AIAA Paper 76-327, San Diego, Calif., July 1976.

[14]Traci, R. M., Albano, E. D., and Farr, J. L., "Perturbation Method for Transonic Flows about Oscillating Airfoils," *AIAA Journal*, Vol. 14, Sept. 1976, pp. 1258-1266.

[15]Ballhaus, W.F. and Goorjian, P.M., "Implicit Finite Difference Computations of Unsteady Transonic Flows about Airfoils Including the Treatment of Irregular Shock-Wave Motions," AIAA Paper 77-205, Los Angeles, Calif. Jan. 1977.

[16]Isogai, K., "Calculations of Unsteady Transonic Flow over Airfoils Using the Full Potential Equation," AIAA Paper 77-448, San Diego, Calif., March 1977.

[17]Ballhaus, W. F. and Goorjian, P. M., "Computation of Unsteady Transonic Flows by the Indicial Method," AIAA Paper 77-447, San Diego, Calif., March 1977.

[18]Rizzetta, D. P., "Transonic Flutter Analysis of a Two-Dimensional Airfoil," AFFDL-TM-77-64-FBR, July 1977.

[19]Scanlan, R. H. and Rosenbaum, R., *Introduction to the Study of Aircraft Vibration and Flutter*, Dover, New York, 1968, pp. 192-201.

[20]Landahl, M. T., *Unsteady Transonic Flow*, Pergamon Press, New York, 1961, p. 4.

[21]Isaacson, E. and Keller, H. B., *Analysis of Numerical Methods*, Wiley, New York, 1966, pp. 384-393.

[22]Beliveau, J., "Eigenrelations in Structural Dynamics," *AIAA Journal*, Vol. 15, July 1977, pp. 1039-1041.

[23]Murman, E. M. and Cole, J. D., "Calculations of Plane Steady Transonic Flows," AIAA Paper 70-188, New York, N.Y., June 1970.